Biomaterials 34 (2013) 9496–9508

Contents lists available at ScienceDirect

Biomaterials

journal homepage: www.elsevier.com/locate/biomaterials

CGKRK-modified nanoparticles for dual-targeting drug delivery to tumor cells and angiogenic blood vessels

Quanyin Hu [a, 1], Xiaoling Gao [b, 1], Ting Kang [a], Xingye Feng [a], Di Jiang [a], Yifan Tu [a], Qingxiang Song [b], Lei Yao [b], Xinguo Jiang [a], Hongzhuan Chen [b], Jun Chen [a, *]

[a] Key Laboratory of Smart Drug Delivery, Ministry of Education, School of Pharmacy, Fudan University, Lane 826, Zhangheng Road, Shanghai 201203, PR China

[b] Department of Pharmacology, Institute of Medical Sciences, Shanghai Jiaotong University School of Medicine, 280 South Chongqing Road, Shanghai 200025, PR China

ARTICLE INFO

Article history:
Received 8 August 2013
Accepted 1 September 2013
Available online 17 September 2013

Keywords:
CGKRK peptide
Paclitaxel
Nanoparticle
Dual-targeting
Antiangiogenic therapy

ABSTRACT

Antiangiogenic therapy shows great advantages in clinical cancer treatment while no overall survival has been achieved. The compromised results were mainly contributed by intrinsic/acquired antiangiogenic drug resistance and increased local invasion or distant metastasis after antiangiogenic therapy. Here we constructed a CGKRK peptide-modified PEG-co-PCL nanoparticulate drug delivery system (DDS), aiming at targeting both tumor angiogenic blood vessels and tumor cells to achieve enhanced anti-tumor activity as well as holding a great potential to overcome the drawbacks of antiangiogenic therapy alone. The obtained CGKRK-functionalized PEG-co-PCL nanoparticles (CGKRK-NP) with a particle size of 117.28 ± 10.42 nm and zeta potential of −15.7 ± 3.32 mV, exhibited an enhanced accumulation via an energy-dependent, lipid raft/caveolae-mediated endocytosis with the involvement of microtubules in human umbilical vein endothelial cells (HUVEC) and an energy-dependent, lipid raft/caveolae-mediated endocytosis with the participation of Golgi apparatus in human U87MG cells. Using coumarin-6 as the fluorescence probe, in vitro U87MG tumor spheroids assays showed that CGKRK-NP effectively penetrated into the tumor spheroids. Selective accumulation and extensive bio-distribution of CGKRK-NP at tumor site was confirmed by in vivo imaging and tumor section analysis. After drug loading, CGKRK-NP enhanced cytotoxicity and apoptosis induction activity of the loaded PTX on both HUVEC cells and U87MG cells and improved its inhibition effect on the growth of U87MG tumor spheroids. The smallest tumor volume was achieved by those mice bearing subcutaneous U87MG tumor following the treatment of PTX-loaded CGKRK-NP. The findings here indicated that CGKRK peptide-functionalized nanoparticulate DDS could be used as an effective tumor angiogenic blood vessels and tumor cells dual-targeting DDS and might provide a great promising approach for reducing the disadvantages of anti-angiogenic therapy alone.

1. Introduction

Angiogenesis, the formation of new blood vessels from pre-existing ones, has been recognized as the distinct hallmark of cancer [1–3]. Many solid tumors depend on an extensive newly formed vascular network to become nourished and to expand [4,5]. Given the role of angiogenesis in tumor growth and progression, targeting tumor vasculature has been proposed as an important strategies for anti-cancer therapy, and inhibition of growth factors/signaling pathways necessary for endothelial cells (ECs) growth and proliferation is one of the practical approaches to inhibit tumor angiogenesis [6]. Tumor vasculature targeting therapy shows great advantages including enhanced "bystander effect" and much easier access to target when compared with conventional chemotherapy that directly kills tumor cells [7,8]. Many antiangiogenic drugs including sorafenib (Nexavar, Bayer/Onyx) [9] and sunitinib (Sutent, Pfizer) [10] had been approved for clinical use since FDA (Food and Drug Administration) approved the first antiangiogenic drug (bevacizumab) for treatment of metastatic colorectal cancer in 2004 [11].

Though angiogenesis inhibitors suppressing tumor growth have been proven to be efficacious in pre-clinical animal models and in

* Corresponding author. Tel.: +86 21 51980066.
E-mail addresses: chenjun_1974@yahoo.com.cn, chenjun@fudan.edu.cn (J. Chen).
[1] Authors contributed equally.

0142-9612/$ – see front matter © 2013 Elsevier Ltd. All rights reserved.
http://dx.doi.org/10.1016/j.biomaterials.2013.09.001

clinical use [12,13], the clinical benefits obtained in terms of overall survival have been more modest than expected. The compromised outcome is mainly caused by two reasons. One is the intrinsic or acquired antiangiogenic drug resistance mediated largely by the tumor microenvironment which can release alternative angiogenic factors such as FGF2 [14], Bv8 [15], G-CSF [16], PDGFC [17] and HGF [18] to preserve the development of blood vessels and play important roles in mediating resistance to antiangiogenic therapy after down-regulation of VEGF. These factors released by cancer cells, stromal cells or both cell types in tumor mass can result in insufficient intracellular drug concentration to kill ECs [19,20]. The other is that antiangiogenic therapy may concomitantly elicit malignant progression of tumors to increased local invasion and distant metastasis [21,22]. Notably, like most systemic chemotherapies, antiangiogenic therapy have not produced enduring efficacy in terms of either tumor shrinkage or long-term survival. Tumor angiogenesis blood vessels and tumor cells dual-targeting chemotherapy offers an alternative option and might achieve great therapeutic efficacy as it can not only destroy the tumor blood vessels and cut off the supply of nutrition and oxygen to tumor [23], but also directly kill tumor cells, holding great potential in reducing acquired drug resistance and metastasis after antiangiogenic therapy [24].

CGKRK peptide, which was discovered by phage display [25], was found to specially bind to both neovascular endothelial cells and tumor cells with high affinity [26]. The receptor of CGKRK peptide was reported to be heparan sulfate—a sulfated polysaccharide which was found on the surface of neovascular endothelial cells and tumor cells [27]. Previous studies showed that intravenous injected CGKRK peptides specifically recognized the vessels in most tumors but not those in normal tissues [28]. Besides, the high cellular internalization contributed by the transmembrane effect of CGKRK peptide made it more favorable for antitumor drug delivery. Unlike cell-penetrating peptides such as TAT peptide which underwent an energy-independent transmembrane process and showed no selectivity between normal cells and tumor cells [29], CGKRK peptide mediated cellular internalization in an energy and heparan sulfate receptor-dependent manner and exhibited high binding selectivity to neovascular endothelial cells and tumor cells [26]. Therefore, here we hypothesized that CGKRK peptide might serve as an efficient ligand that can simultaneously deliver its payload to both tumor endothelial cells and tumor cells to enhance anti-cancer activity.

CGKRK peptide was functionalized to PEG-co-PCL nanoparticles via a maleimide-thiol coupling reaction aiming at obtaining precise dual-targeting efficacy. Using HUVEC cells as the model of neovascular endothelial cells and U87MG cells as the model of tumor cell model (both HUVEC cells and U87MG cells overexpressed heparan sulfate), cellular association and internalization mechanism was investigated on HUVEC cells and U87MG cells as well as penetration ability on U87MG tumor spheroids by using coumarin-6 as the fluorescence probe. In vivo bio-distribution of functionalized PEG-co-PCL nanoparticles was studied by taking DiR as near-infrared (NIR) probe. After encapsulating paclitaxel (PTX) as the model drug, the anti-tumor efficacy of CGKRK-NP was evaluated on in vitro U87MG tumor spheroids and in vivo subcutaneous U87MG tumor-bearing mice.

2. Materials and methods

2.1. Materials

CGKRK peptides were synthesized by ChinaPeptides Co., Ltd (Shanghai, China), purified by HPLC and verified for purity ≥98%. Methoxypoly(ethylene glycol) $_{3000}$-poly(ε-caprolactone) $_{20000}$ (MePEG-PCL) and maleimide-poly(ethylene glycol) $_{3400}$-poly(ε-caprolactone) $_{20000}$ (Male-PEG-PCL) were kindly provided by East China University of Science and Technology. Coumarin-6, DiR (1, 1′-dioctadecyl -3, 3, 3′, 3′-tetramethyl indotricarbocyanine Iodide) and Hoechst 33258 were provided by Sigma–Aldrich (St. Louis, MO, USA). DAPI (4, 6-diamidino-2-phenylindole) was purchased from Molecular Probes (Eugene, OR, USA), cell counting kit-8 (CCK-8) from Dojindo Laboratories (Kumamoto, Japan) and Annexin V-FITC Apoptosis Detection kit from BD PharMingen (Heidelberg, Germany). PTX was obtained from Xi'an Sanjiang Biological Engineering Co. Ltd (Xi'an, China) and Taxol® from Bristol-Myers Squibb Company. Alexa Fluor® 647 anti-mouse CD31 Antibody was purchased from Biolegend (San Diego, CA, USA). All the other solvents were purchased from Sinopharm Chemical Reagent Co., Ltd (Shanghai, China) and were of analytical or chromatographic grade.

Dulbecco's Modified Eagle Medium (DMEM) (high glucose) cell culture medium, certified fetal bovine serum (FBS), penicillin/streptomycin stock solutions and 0.25% Trypsin-EDTA were all obtained from Invitrogen Co., USA.

2.2. Cells and animals

Primary human umbilical vein endothelial cells (HUVEC cells) were purchased from Cascade Biologics (USA) and Human U87MG cell lines were provided by Cell Institute of Chinese Academy of Sciences (Shanghai, China). Both HUVEC cells and U87MG cells were cultured in DMEM containing 10% fetal bovine serum, 100 U/ml penicillin and 100 μg/ml streptomycin at 37 °C in a 5% CO_2/95% air humidified environment incubator (Thermo HERAcell®, USA). All experiments were performed in the logarithmic phase of cell growth.

Balb/c nude mice (male, 4–5 weeks, 20 ± 2 g) were obtained from Experimental Animal Center of Fudan University and housed at 25 ± 1 °C with access to food and water ad libitum. The protocol of animal experiments was approved by the Animal Experimentation Ethics Committee of Fudan University.

2.3. Preparation of CGKRK-NP

Unmodified nanoparticles (NP) loaded with PTX were prepared with a blend of Maleimide-PEG-PCL and MePEG-PCL using the emulsion/solvent evaporation technique as described previously [30]. Briefly, the mixture of PTX (0.25 mg), Maleimide-PEG-PCL (2.5 mg) and MePEG-PCL (22.5 mg) was dissolved in 1 mL dichloromethane, followed by the condition of 2 mL of 1% sodium cholate and then applied to ultrasonication for 2.4 min at 280 W using probe sonicator (Ningbo Scientz Biotechnology Co. Ltd., China) under ice bath. Thereafter, the resulting O/W emulsion was diluted into 8 mL of 0.5% sodium cholate aqueous solution under rapid magnetic stirring for 5 min. After evaporating dichloromethane at room temperature with a ZXB98 rotavapor (Shanghai Institute of Organic Chemistry, China), the obtained NPs were centrifuged at 15,000 rpm for 1 h using T J-25 centrifuge (Beckman Counter, USA). The nanoparticles were resuspended in 0.01 M HEPES buffer (pH 7.0) for further used with the supernatant discarded.

CGKRK peptide-modified NPs (CGKRK-NP) were prepared via a maleimide-thiol coupling reaction. For the conjugation with CGKRK peptide, the NPs and CGKRK peptide were subjected to a container and stirred at room temperature for 6 h at the molar ratio of CGKRK peptide to maleimide-PEG-PCL 3:1. The products were then eluted with distilled water through the 1.5 × 20 cm sepharose CL-4B column (Pharmacia Biotech, Inc., Sweden) to remove the unconjugated peptides.

2.4. Characterization of NP and CGKRK-NP

Particle size and zeta potential of NP and CGKRK-NP were determined by dynamic light scattering detector (Zetasizer, Nano-ZS, Malvern, UK). The morphological examination of NPs was performed on a transmission electron microscope (TEM) (H-600, Hitachi, Japan) following negative staining with sodium phosphotungstate solution. In order to verify the surface modification of nanoparticle with CGKRK peptide, the NP samples were lyophilized via an ALPHA 2-4 Freeze Dryer (0.070 Mbar Vacuum, −80 °C, Martin Christ, Germany) and then subjected to X-ray photoelectron spectroscopy (XPS) analysis via a RBD upgraded PHI-5000C ESCA system (Perkin Elmer) to determine the surface composition.

To determine the encapsulation efficiency (EE) and loading capacity (LC) of NP-PTX and CGKRK-NP-PTX, the NP samples were dissolved in acetonitrile and subsequently analyzed on an Agilent 1100 HPLC system (Agilent Technologies, CA, USA) with the detection wavelength of 227 nm. The encapsulation efficiency (EE) and loading capacity (LC) were calculated as indicated below ($n = 3$).

$$\mathrm{EE}(\%) = \frac{\text{Amount of PTX in the nanoparticles}}{\text{Total amount of PTX added}} \times 100\%$$

$$\mathrm{LC}(\%) = \frac{\text{Amount of PTX in the nanoparticles}}{\text{nanoparticles weight}} \times 100\%$$

2.5. In vitro PTX release

In vitro PTX release from nanoparticles was determined under different pH conditions (pH 7.4 and 6.0 representing the physiologic pH and pH in the tumor microenvironment, respectively). The experiment was performed using an equilibrium dialysis method with phosphate buffer solution (PBS, pH 7.4 and 6.0, with 0.1% Tween-80 to provide sink condition) as the release media [31]. Briefly, 1 mL of

Table 1
Characterization of NP and CGKRK-NP. Data represented mean ± SD ($n = 3$).

Nanoparticles	Particle size (nm)	Polydispersity index (PI)	Zeta potential (mV)
NP	103.13 ± 5.7	0.096 ± 0.017	−32.7 ± 5.63
CGKRK-NP	117.28 ± 10.42	0.170 ± 0.07	−15.7 ± 3.32

Taxol®, PTX-loaded NP and CGKRK-NP formulation with the concentration of PTX adjusted to 100 μg/ml were subjected to a dialysis bag (MWCO = 8000 Da, Greenbird Inc., Shanghai, China) and sealed. Following immediately immersed in 30 mL of release medium, the mixture was incubated at 37 °C at the shaking speed of 120 rpm. Then at every pre-determined time points (0.5, 1, 2, 3, 4, 6, 8, 12, 24, 36, 48, 72 and 96 h), a 0.2 mL of the release sample was withdrawn and immediately an equal volume of fresh dissolution medium were replenished. The samples were subjected to HPLC analysis later as described previously [32].

2.6. Cellular association and uptake of NPs in HUVEC and U87MG cells

The cellular association measurement was performed via both fluorescent microscopy and KineticScan HCS analysis. For qualitative analysis, HUVEC cells and U87MG cells were seeded in a 24-well plate at the density of 5×10^4 cells/well and allowed to attach for 24 h, respectively. Then the cells were exposed to coumarin-6-labeled NP and CGKRK-NP at the nanoparticle concentrations ranged from 25 μg/ml to 200 μg/ml. One hour later, the cells were washed twice with PBS (pH 7.4), fixed with 4% formaldehyde for 15 min, stained with DAPI for 15 min and subjected to observation under a fluorescent microscopy (Leica DMI4000 B, Germany).

For quantitative study, HUVEC cells and U87MG cells were cultured on a 96-well plate at the density of 5×10^3 cells/well. Twenty-four hours later, the cells were treated with NP and CGKRK-NP at the nanoparticle concentrations ranged from 25 μg/ml to 600 μg/ml for 37 °C and 4 °C, respectively. After removing the nanoparticles and washing twice with PBS 1 h later, the cells were then fixed with 4% formaldehyde for 15 min and stained with Hoechst 33258 away from light for 15 min, and then subjected to a KineticScan HCS Reader (Thermo scientific, USA) for analysis. For determining the fluorescent signals from the internalized nanoparticles, the cells were incubated with trypan blue (Beyotime Institute of Biotechnology) to quench those fluorescent signals from the uninternalized nanoparticles, and subjected to a second reading. For evaluating the time related cellular association experiment, the incubation time was ranged from 0.5 h to 4 h at the nanoparticle concentration of 200 μg/ml.

To study the internalization mechanism, both HUVEC cells and U87MG cells were pre-incubated with different endocytosis inhibitors, including 10 μg/ml chlorpromazine, 4 μg/ml colchicines, 10 μg/ml cyto-D, 5 μg/ml BFA, 5 μg/ml filipin, 10 mM NaN_3, 50 mM deoxyglucose, 2.5 mM methyl-β-cyclodextrin (M-β-CD), 200 nM monensin, 20 μM nocodazole, and 100 μg CGKRK peptide, for 1 h. After that, 200 μg/ml coumarin-6-labeled NP and CGKRK-NP were added into each well and incubated for 1 h. Then the cells were treated as described above before quantitative study.

2.7. Penetration of CGKRK-NP in tumor spheroid

For multicellular tumor spheroids formation, U87MG cells were seeded in a 48-well plate pre-coated with 2% (w/v) agarose gel at the density of 2×10^3 cells/well. After cultured for 7 days, the uniform and compact spheroids were selected for further experiments.

In order to study the penetration ability of CGKRK-NP, the spheroids were exposed to coumarin-6-labeled NP and CGKRK-NP at nanoparticle concentration of 400 μg/ml. Four hours later, the tumor spheroids were washed with cold PBS for three times, fixed with 4% formaldehyde for 30 min and then subjected to laser scanning confocal microscopy analysis (LSM510, Leica, Germany).

2.8. Bio-distribution of CGKRK-NP-DiR in tumor-bearing mice

In order to establish U87MG tumor-bearing nude mice model, the suspension of U87MG cells (4×10^6 cells in 200 μl cell culture medium) were injected into the subcutaneous tissue of the right hind legs. The subcutaneous tumors were allowed to grow up to 0.6–0.8 cm in diameter for further use.

The bio-distribution of CGKRK-NP in U87MG tumor-bearing mice following intravenous administration was studied via a CRi in vivo imaging system (CRi, MA, USA). Six mice were randomly divided into two groups and intravenously injected DiR-labeled NP and CGKRK-NP at the dose of 1 mg/kg DiR. The fluorescent images were taken at the pre-determined time points (2, 4, 6, 8, 12 h). Then the tumor-bearing mice were sacrificed with the organs harvested at 24 h post-injection for ex vivo imaging.

2.9. Penetration of CGKRK-NP into tumor interior

U87MG tumor-bearing nude mice model was established as abovementioned and the tumor masses were allowed to grow up to 450 mm^3. After that, the mice were intravenously injected coumarin-6-labeled NP and CGKRK-NP at the equal coumarin-6 dose. Three hours later, the mice were sacrificed and the tumor tissues were harvested, fixed with 4% formaldehyde for 24 h and then dehydrated in 10%, 30% sucrose solution. Afterward, the tumors were imbedded in OCT (Sakura,

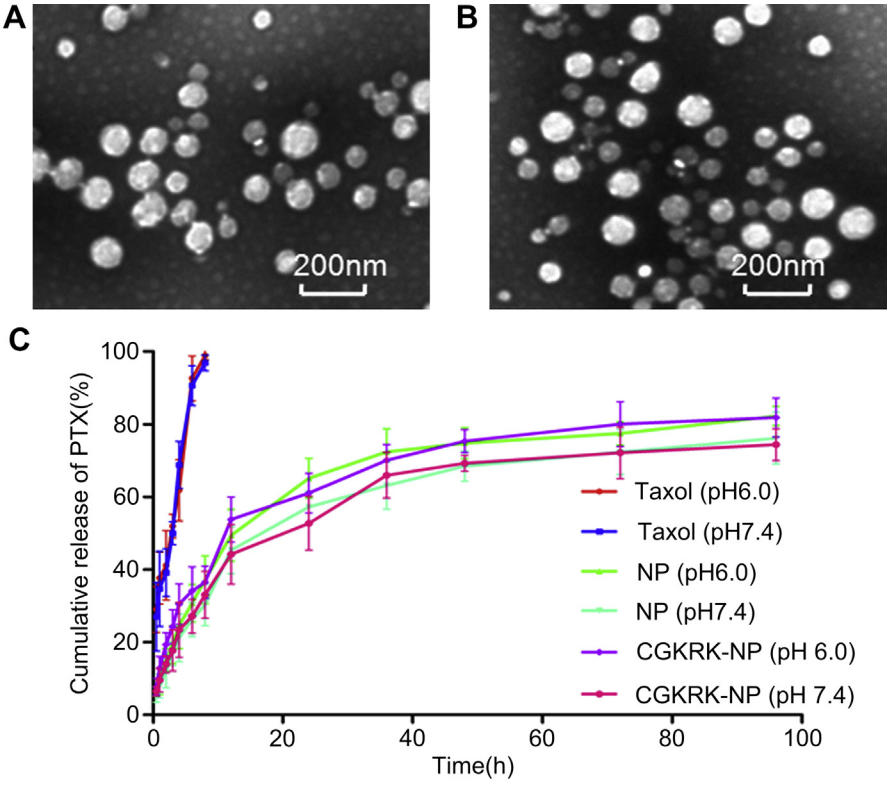

Fig. 1. Characterization of NP and CGKRK-NP. TEM images of NP (A) and CGKRK-NP (B). PTX release profiles from Taxol®, NP-PTX and CGKRK-NP-PTX in PBS (pH 6.0) and PBS (pH 7.4) with 0.1% Tween-80 (C). The bar is 200 nm.

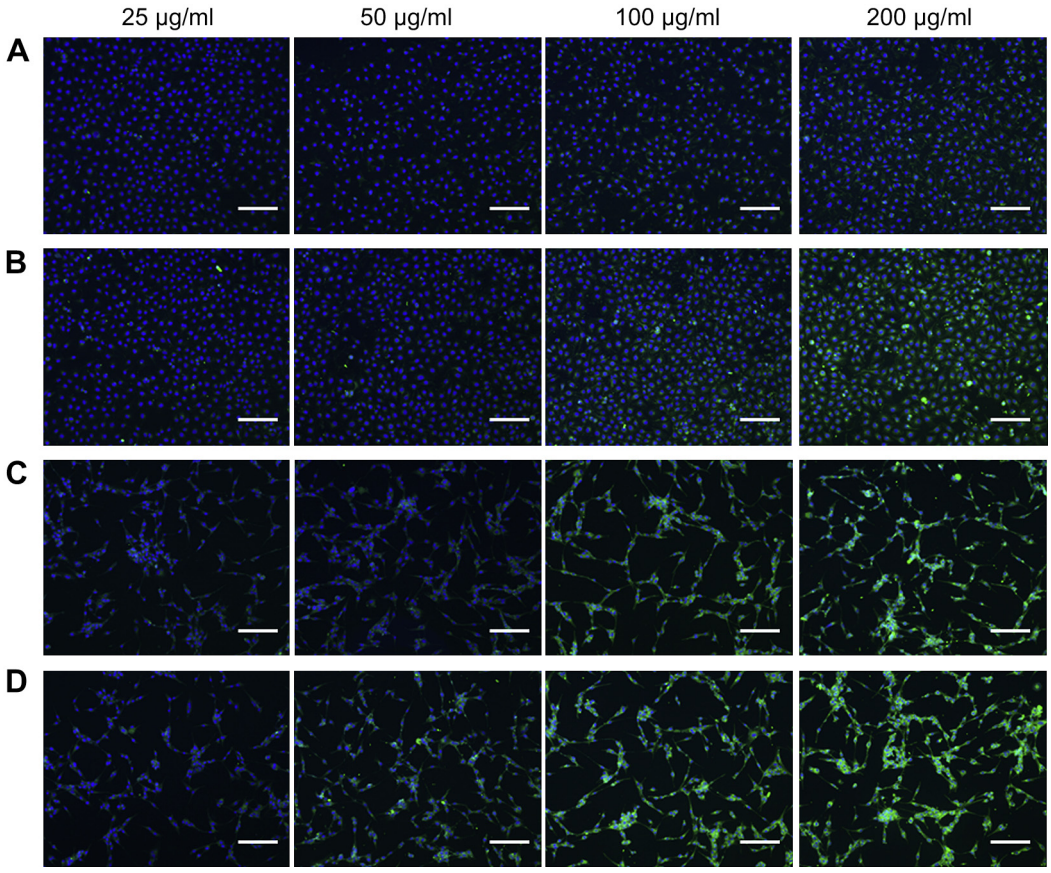

Fig. 2. Cellular association of coumarin-6-labeled unmodified NP and CGKRK-NP in HUVEC cells (A, B) and U87MG cells (C, D) after incubation for 1 h at the concentration ranged from 25 to 200 μg/ml. Green: coumarin-6 labeled nanoparticles. Blue: nuclei. Original magnification: 20×. The bar is 100 μm. (For interpretation of the references to color in this figure legend, the reader is referred to the web version of this article.)

Torrance, CA, USA), frozen at 80 °C and sectioned at 7 μm. For immunostaining, the slides were firstly blocked with 20% goat serum for 1 h at room temperature, and then incubated with Alexa Fluor® 647 anti-mouse CD31 antibody overnight at 4 °C. Finally, the slides were stained with DAPI and subjected to confocal microscopy analysis (LSM710, Leica, Germany).

2.10. Cell apoptosis assay

Both HUVEC cells and U87MG cells (5×10^5 cells/well) were seeded in a 6-well plate and allowed to grow for 24 h. After that, the cultured medium was substituted with 100 ng/ml different PTX formulations including Taxol®, NP-PTX and CGKRK-NP-PTX and incubated for 48 h. For qualitative analysis, the cells were washed with PBS, fixed with 4% formaldehyde for 15 min and stained with DAPI for nuclear morphology observation via a fluorescent microscope (Leica DMI4000 B, Germany). For quantitative apoptosis assay, the treated cell were trypsinized, centrifuged at 1000 g for 5 min, and then stained with FITC Annexin V Apoptosis Detection Kit I (Becton Dickinson Medical Devices, Shanghai, China) according to the manufacture's protocol. After that, the cells undergoing apoptosis were quantified by a FACSscan Flow Cytometer (BD PharMingen, Heidelberg, Germany). The cells treated with DMEM were used as control.

2.11. Anti-proliferation assay

The anti-proliferation activity of CGKRK-NP-PTX on both HUVEC cells and U87MG cells was evaluated by using the CCK-8 assay. Briefly, the cells were seeded in 96-well plates at the density of 2×10^5 cells/well. Twenty-four hours later, Taxol®, NP-PTX and CGKRK-NP-PTX were added into wells at the PTX concentration ranged from 1 ng/ml to 1 μg/ml, respectively. Seventy-two hours later, 10 μl CCK8 was added into each well and incubated for 1 h. After that, the plates were subjected to a microplate reader (Thermo Multiskan MK3, USA) for cell viability assay at the wavelength of 450 nm.

2.12. Inhibition of tumor spheroid growth

The anti-growth ability of CGKRK-NP loaded with PTX on tumor spheroids was evaluated by measuring the size of spheroids following different PTX formulations treatment. Briefly, the selected tumor spheroids (6 days incubation) were treated with Taxol®, NP-PTX and CGKRK-NP-PTX at PTX concentration of 200 ng/ml every other day for a week. The size of tumor spheroids was carefully observed under an invert microscope (Chongqing Optical & Electrical Instrument, Co., Ltd., Chongqing, China). The spheroids treated with DMEM were used as the negative control.

2.13. In vivo anti-tumor growth effect of CGKRK-NP-PTX

In vivo anticancer activity was evaluated in mice bearing subcutaneous U87MG tumor. The treatment schedule started when the tumor volume reached approximate 100 mm^3. The mice were randomly divided into four groups ($n = 6$) and treated with Taxol®, NP-PTX and CGKRK-NP-PTX via tail vein injection on the day 0, 2, 4 and 6 (PTX dosage: 5 mg/kg, mice treated with physiological saline were used as control). Tumor size was monitored via serial caliper measurement every 2 days and the tumor volume was estimated using the formula: Volume $= 0.5 \times$ length $\times$ $(\text{width})^2$. On the day 14, the animals were sacrificed by cervical dislocation, and the tumor mass was harvested, weighted and photographed.

2.14. Statistical analysis

All the data were presented as mean ± standard deviation. Unpaired student's *t* test was used for between two-group comparison and one-way ANOVA with Bonferroni tests for multiple-group analysis. Statistical significance was defined as $p < 0.05$.

3. Results

3.1. Characterization of nanoparticles

The nanoparticles prepared from a blend of Maleimide-PEG-PCL and MePEG-PCL with the emulsion/solvent evaporation method exhibited the sizes of 102.81 ± 5.32 nm. After modified with CGKRK peptides, the size slightly increased to 115.34 ± 7.83 nm with the same narrow size distribution (Table 1). Representative TEM photographs illustrated that NP and CGKRK-NP exhibited the same

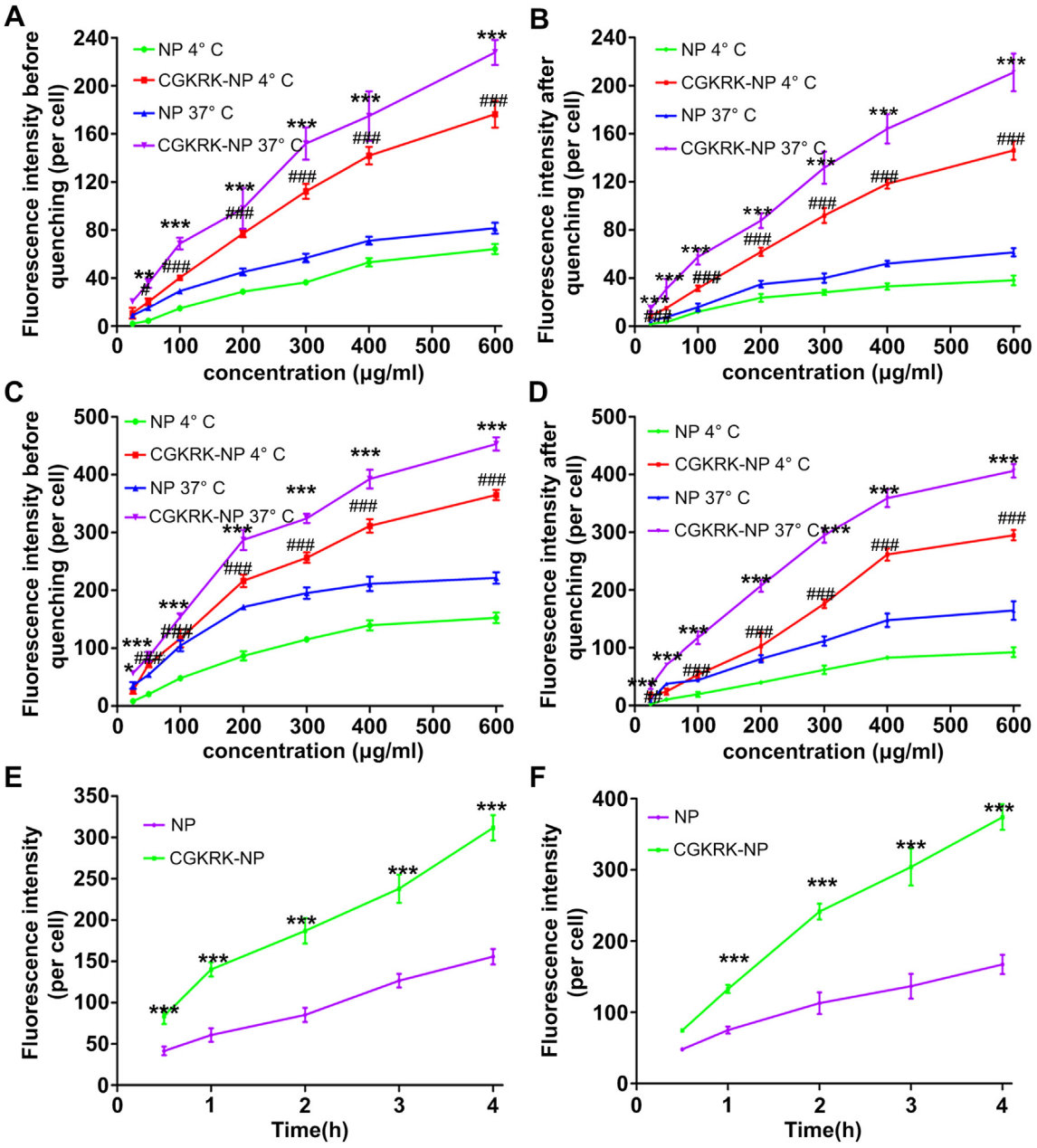

Fig. 3. Cellular association and uptake of coumarin-6-labeled unmodified NP and CGKRK-NP at different temperature (4 °C and 37 °C) after incubation for 1 h at the nanoparticle concentrations from 25 μg/ml to 600 μg/ml in HUVEC cells (A, B) and U87MG cells (C, D). Cellular association of coumarin-6-labeled unmodified NP and CGKRK-NP at different incubation time ranged from 0.5 to 4 h in HUVEC cells (E) and C6 cells (F) at nanoparticles concentration of 200 μg/ml $^{*}p < 0.05$, $^{**}p < 0.01$, $^{***}p < 0.001$ significantly higher than the cellular uptake of unmodified NP at 37 °C, and $\#p < 0.05$, $\#\#p < 0.01$, $\#\#\#p < 0.001$ higher than the cellular uptake of unmodified NP at 4 °C.

spherical shape (Fig. 1A and B). Zeta potential of NP formulations was −32.7 ± 5.63 mV, while that of CGKRK-NP was −15.7 ± 3.32 mV.

XPS assay showed that the surface nitrogen detected on CGKRK-NP was 0.47% while that on the surface of unconjugated NP was undetectable.

The EE of the optimized NP and CGKRK-NP was 47.67 ± 3.21% and 46.54 ± 4.76%, respectively, with the LC 0.94 ± 0.09% and 0.92 ± 0.87%, respectively.

3.2. In vitro PTX release

In vitro PTX release experiment was performed in PBS at different PH (PH 7.4 and PH 6.0). pH 7.4 and pH 6.0 represented the physiologic pH and pH in the tumor microenvironment respectively. As shown in Fig. 1C, a burst release was achieved for Taxol® in both PH 6.0 and PH 7.4 PBS with over 98% cumulative release of PTX within 6 h. While NP-PTX and tLyp-1-NP-PTX presented almost the same controlled release behavior, achieving cumulative PTX release 76.18 ± 7.15% and 74.38 ± 4.36%, respectively, after 96 h incubation in PBS (pH 7.4). The release rate of NP-PTX and tLyp-1-NP-PTX in PH 6.0 PBS was faster than that in PH 7.0 PBS (82.27 ± 2.58% for NP-PTX and 81.84 ± 5.36% after 96 h incubation).

3.3. Cellular association and uptake of NPs in HUVEC cells and U87MG cells

The cellular association of NPs was characterized by both fluorescent microscopy and HCS Reader analysis by using coumarin-6

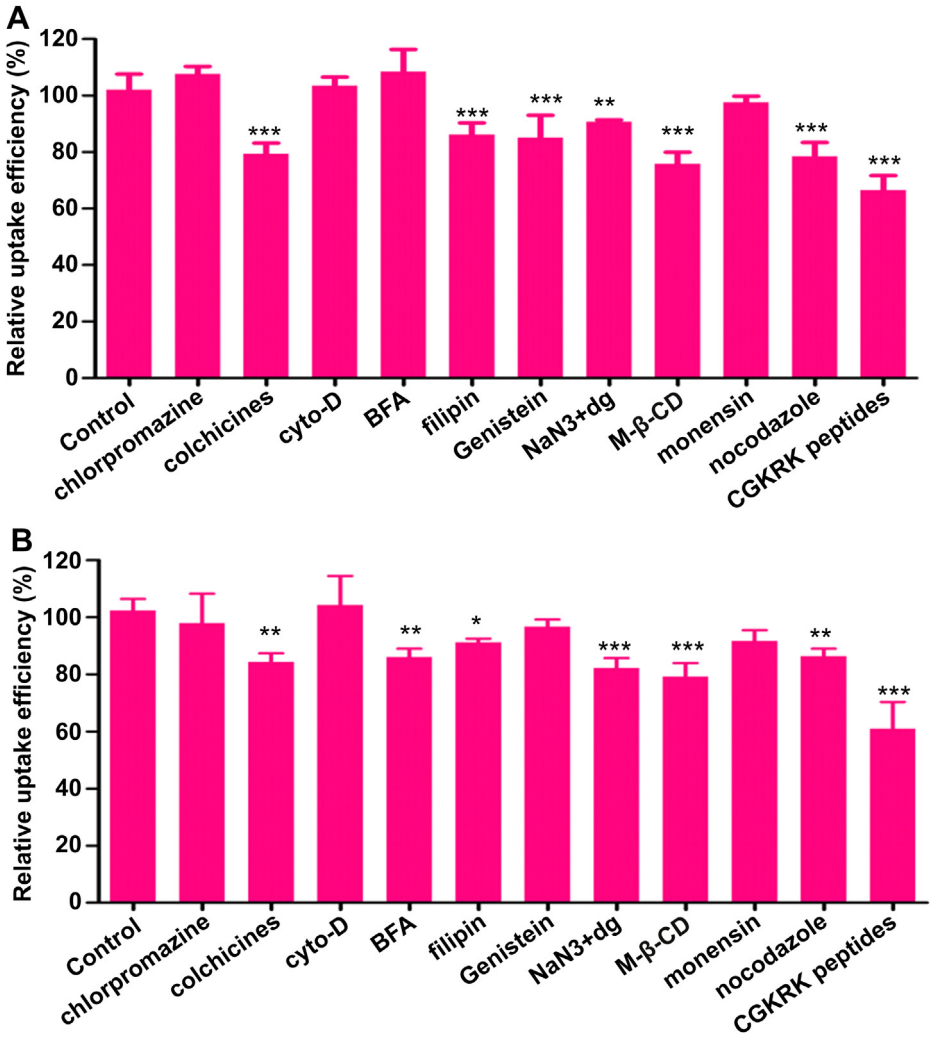

Fig. 4. Cellular uptake of coumarin-6 labeled CGKRK-NP in the presence of different endocytosis inhibitors in HUVEC cells (A) and U87MG cells (B). Fluorescence intensity in the non-inhibited cells was used as control. Data represented mean ± SD ($n = 3$). $^{*}p < 0.05$, $^{**}p < 0.01$, $^{***}p < 0.001$ significantly different with that of control.

as the fluorescence probe. For quantitative analysis, as shown in Fig. 2, the fluorescence intensity of CGKRK-NP was much higher than that of unconjugated NP on both HUVEC cells and U87MG cells at the nanoparticles concentration ranged from 25 μg/ml to 200 μg/ml.

Quantitative analysis confirmed the concentration-dependent cellular association of NP and CGKRK-NP in both HUVEC cells and U87MG cells. Besides, the cellular association of CGKRK-NP on both cells was much greater than that of NP at 37 °C and 4 °C (Fig. 3A–D). The cellular association of CGKRK-NP was 2.3, 2.2, 2.7, 2.5, 2.8 folds higher on HUVEC cells and 1.5, 1.7, 1.8, 1.8, 2.0 folds higher on U87MG cells when compared with that of NP at 37 °C at the nanoparticles concentration of 100, 200, 300, 400 and 600, respectively. While after quenching by trypan blue staining, the cellular uptake of CGKRK-NP was 3.65, 2.54, 3.30, 3.10, 3.30 folds higher in HUVEC cells and 2.67, 2.55, 2.63, 2.43, 2.50 folds higher in U87MG cells when compared with that of NP at 37 °C at the nanoparticles concentration of 100, 200, 300, 400 and 600, respectively. In addition, the time-related experiment exhibited that the fluorescence intensity of CGKRK-NP on both HUVEC cells and U87MG cells was significantly enhanced when compared with that of NP at all experiment time points (Fig. 3E, F).

Endocytosis inhibition experiment showed that the cellular uptake of CGKRK-NP was inhibited by colchicines ($P < 0.001$), filipin ($P < 0.001$), Genistein ($P < 0.001$), NaN_3 + dg ($P < 0.01$), M-β-CD ($p < 0.001$) and nocodazole ($p < 0.001$) in HUVEC cells and restricted by colchicines ($P < 0.05$), BFA ($P < 0.05$), filipin ($P < 0.05$), NaN_3 + dg ($P < 0.001$) and nocodazole ($p < 0.01$) in U87MG cells when compared with non-inhibition control (Fig. 4). Meanwhile, the pre-added 100 μg CGKRK peptide decreased the association of CGKRK-NP by 82.47% ($P < 0.001$) and 70.9% ($P < 0.001$) on HUVEC cells and U87MG cells, respectively.

3.4. Penetration of CGKRK-NP in tumor spheroid

The multicellular U87MG tumor spheroids were employed to evaluate the penetration ability of CGKRK-NP. As shown in Fig. 5, the penetration depth of unmodified NP was 87.72 μm and the fluorescence mostly located at the edge of spheroid, while that of CGKRK-NP distributed more extensive and penetrated much deeper with the distance of 108.36 μm in multicellular tumor spheroids.

3.5. Bio-distribution of CGKRK-NP in tumor-bearing mice

In vivo CGKRK-NP targeting ability was determined on subcutaneous U87MG tumors-bearing mice via a small animal imaging system. The mice followed by CGKRK-NP-DiR injection exhibited a much stronger fluorescence intensity at tumor site at every imaging

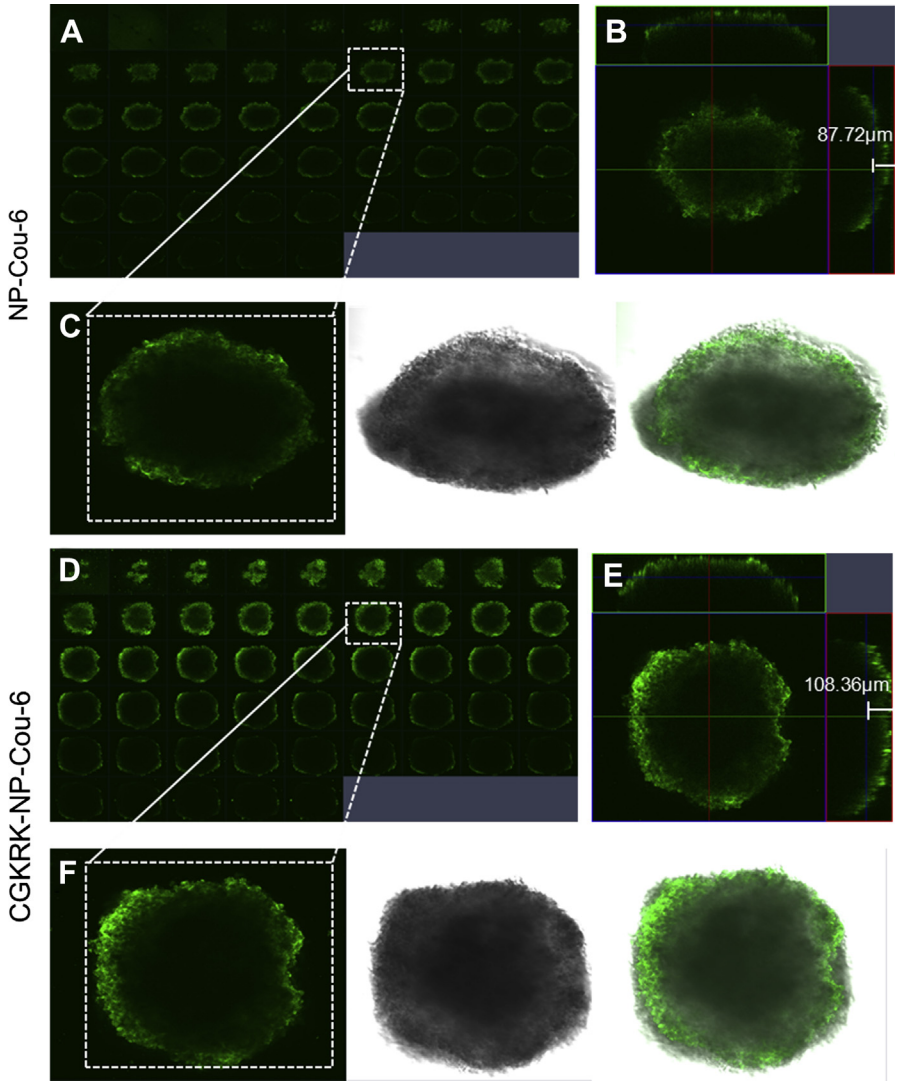

Fig. 5. Penetration of coumarin-6-labeled NP and CGKRK-NP in U87MG tumor spheroids. Multi-level scan started the top of the spheroid in 5 μm intervals of the penetration of NP (A) and CGKRK-NP (D). Amplification, bight field and merge of fluorescent images of NP (C) and CGKRK-NP (F). Quantitative analysis of the penetration depth of NP (B) and CGKRK-NP (E).

time (2, 4, 6, 8, 12 h) when compared with that of NP group (Fig. 6A, B). Ex vivo imaging of organs 24 h post-injection also confirmed that CGKRK modification led to much more accumulation of nanoparticles in tumor sites (Fig. 6C).

3.6. Penetration of CGKRK-NP into tumor interior

In order to evaluate …, frozen tumor section was prepared and observed under the confocal microscope. Using … for…, it was found that a low accumulation of coumarin-6-labeled NP was observed in tumor site, mostly trapped in the blood vessels and did not get into tumor parenchyma (Fig. 7A). In contrast, obvious stronger fluorescence signals from CGKRK-NP was observed around the blood vessels and many extravasated from vessels and penetrated into tumor foci (Fig. 7B).

3.7. Cell apoptosis assay

Both HUVEC cells and U87MG cells was used to study the cell apoptosis induced by different PTX formulations. Paclitaxel formulated in Taxol®, NP-PTX and CGKRK-NP-PTX activated apoptosis in both HUVEC cells and U87MG cells with fragmented nuclei observed after treated for 48 h. In addition, the nuclei of both cells treated with CGKRK-NP-PTX became severely fragmented with the unsharp borders (Fig. 8A, C).

Quantitative flow cytometry results confirmed that the ability of the different PTX formulations to induce cell apoptosis followed the order: CGKRK-NP-PTX > NP-PTX > Taxol® (Fig. 8B, D). The percentage of early apoptosis treated with CGKRK-NP-PTX (18.35 ± 2.3% and 22.25 ± 3.1% for HUVEC cells and U87MG cells, respectively) was much higher than that treated with NP-PTX (10.19 ± 1.6% and 9.46 ± 2.3% for HUVEC cells and U87MG cells, respectively) and Taxol® (8.89 ± 1.3% and 8.65 ± 1.9% for HUVEC cells and U87MG cells, respectively).

3.8. Anti-proliferation assay

The anti-proliferation of different PTX formulations were evaluated on both HUVEC cells and U87MG cells by using CCK8 method. As shown in Fig. 9, CGKRK-NP exhibited much higher toxicity (IC50 values of 96.95 ng/ml and 52.51 ng/ml on HUVEC cells and U87MG cells, respectively) when compared with NP

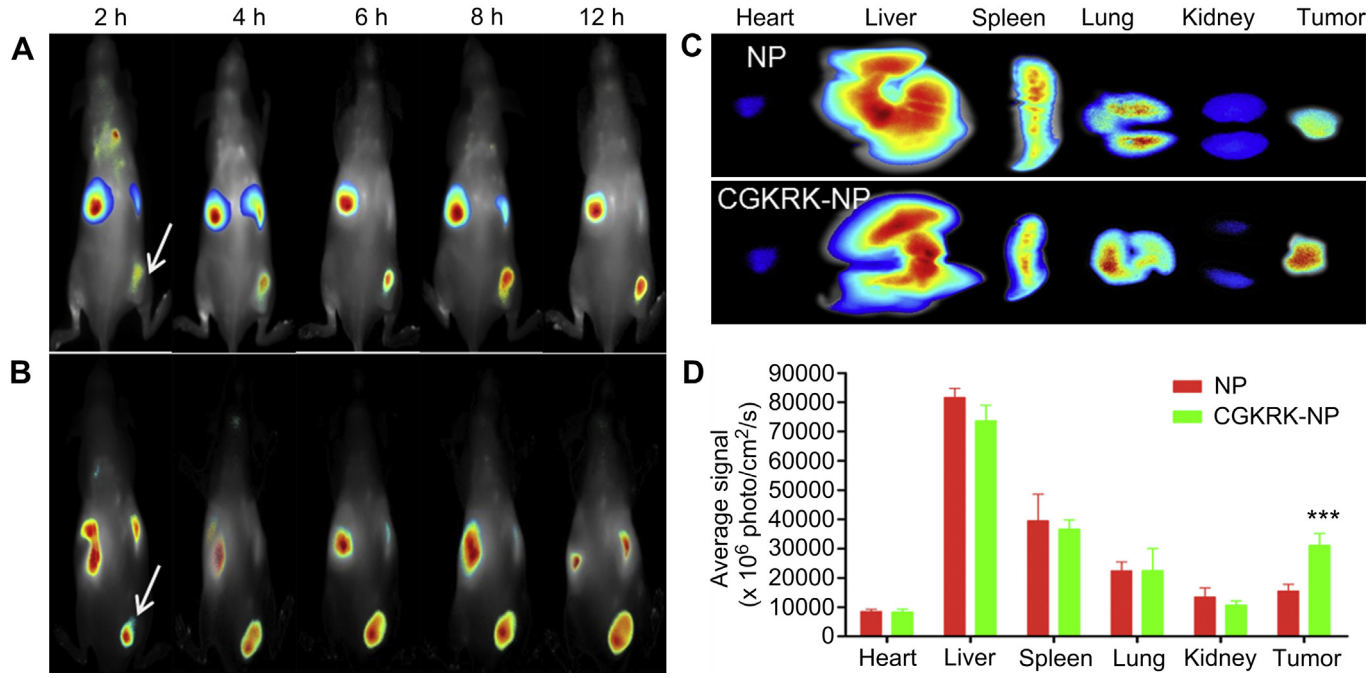

Fig. 6. In vivo near-infrared imaging of mice bearing subcutaneous U87MG tumors intravenously treated with 200 μl DiR-labeled NP (A) and CGKRK-NP (B) through the tail vein at 2 h, 4 h, 6 h, 8 h, 12 h, respectively. Ex vivo fluorescence imaging of dissected organs after 24 h post-injection (C). Semi-quantitative analysis of the fluorescent intensity of NP-DiR and CGKRK-NP-DiR in different organs and tumors (D). Data represented mean ± SD ($n = 3$). $^{*}p < 0.05$, $^{**}p < 0.01$, $^{***}p < 0.001$ significantly different with that of NP. All the arrows represented the site of tumor.

(163.1 ng/ml and 107.3 ng/ml for HUVEC cells and U87MG cells, respectively) and Taxol® (193.8 ng/ml and 126.0 ng/ml on HUVEC cells and U87MG cells, respectively).

3.9. Inhibition of tumor spheroid growth

The inhibition of tumor spheroids growth was evaluated following the treatment with serum-free DMEM, Taxol®, NP-PTX and CGKRK-NP-PTX at the PTX concentration of 200 ng/ml according to the schedule of every two days for one week. As shown in Fig. 10, the tumor spheroid treated with serum-free DMEM kept growing and became more compact, whereas the spheroids treated with PTX formulations exhibited apoptosis of marginal cells and reduction in sizes. In addition, the tumor spheroid exposed to CGKRK-NP-PTX exhibited the smallest size with loose intercellular junctions and lost three-dimensional structure at day 6 (Fig. 10).

3.10. In vivo anti-tumor growth effect of CGKRK-NP-PTX

The anti-tumor growth effect was evaluated by measuring the tumor volume and weight following the treatment of saline, Taxol®, NP-PTX and CGKRK-NP-PTX at PTX dose of 5 mg/kg every two days for two weeks. As shown in Fig. 11, the ability of different PTX formulations to inhibit tumor growth followed the order: CGKRK-NP-PTX > NP-PTX > Taxol® > Saline. The tumor volume of mice treated with CGKRK-NP-PTX was 0.15 cm^3 at the 14 days post-injection and 2.2, 2.47, 5.87 folds smaller than NP-PTX group, Taxol® group and saline group, respectively. The tumor weight of mice treated with CGKRK-NP-PTX was 0.14 g at the 14 days post-injection and 2.2, 2.86, 5.7 folds lighter than NP-PTX group, Taxol® group and saline group, respectively.

4. Discussion

Antiangiogenic therapy had been recognized as an effective treatment to suppress tumor growth and achieved great development since Judah Folkman's long-standing vision of angiogenesis as a

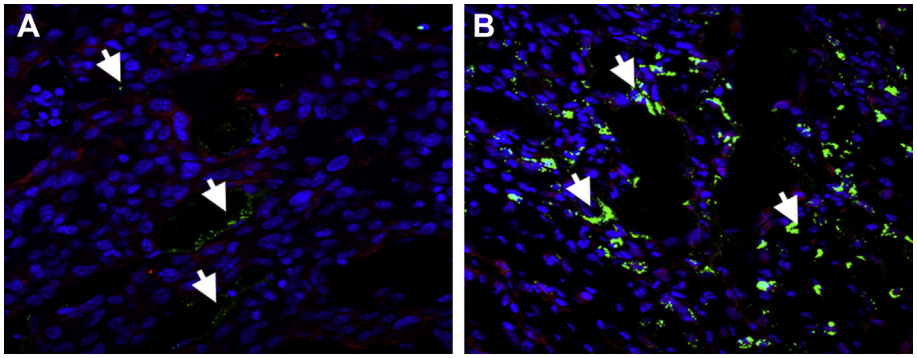

Fig. 7. In vivo tumor distribution of coumarin-6-labeled NP (A) and CGKRK-NP (B) 3 h after administration. Blue: DAPI stained cell nuclei. Green: Coumarin-6-labeled nanoparticles. Red: CD31 stained blood vessels. (For interpretation of the references to color in this figure legend, the reader is referred to the web version of this article.)

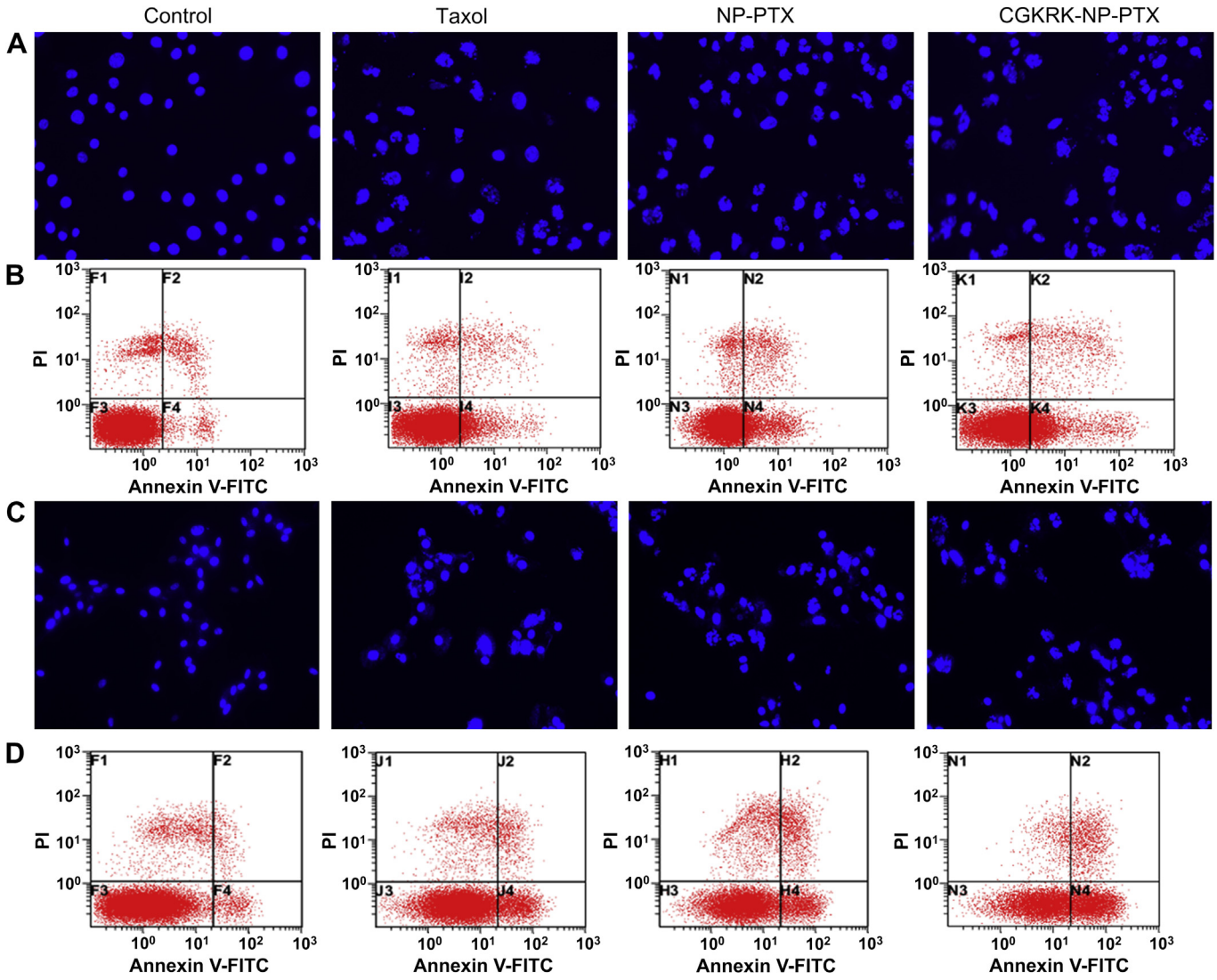

Fig. 8. Induction of apoptosis in HUVEC cells and U87MG cells following 48 h incubation with Taxol®, NP-PTX and CGKRK-NP-PTX (PTX concentration 100 ng/ml). Morphology of nuclei of HUVEC cells (A) and U87MG cells (C) after stained with DAPI. Flow cytometry analysis of apoptosis. The HUVEC cells (B) and U87MG cells (D) were stained with Annexin V-FITC and PI. Both cells incubated with drug-free DMEM served as the control. Original magnification: 20×.

therapeutic target [33,34]. Agents that inhibit vascular endothelial growth factor (VEGF), one of the most potent promoters of angiogenesis, and its receptor have been approved for clinical use [35,36]. However, continued clinical and pre-clinical investigations have identified major drawbacks associated with the application of this class of agents, including inherent/acquired resistance [37,38] and induction of tumor invasiveness and metastasis [39,40]. The main course of these severe drawbacks was that the modified tumor

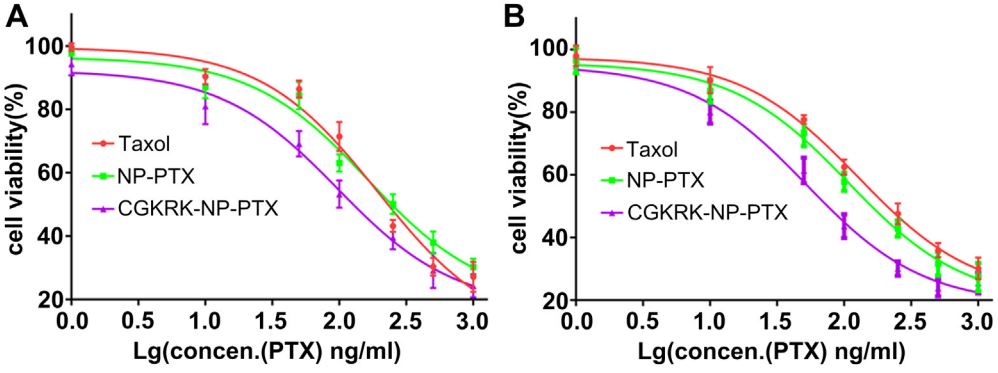

Fig. 9. Cell viability of HUVEC cells (A) and U87MG cells (B) after treated with Taxol®, NP-PTX and CGKRK-NP-PTX for 72 h at 37 °C.

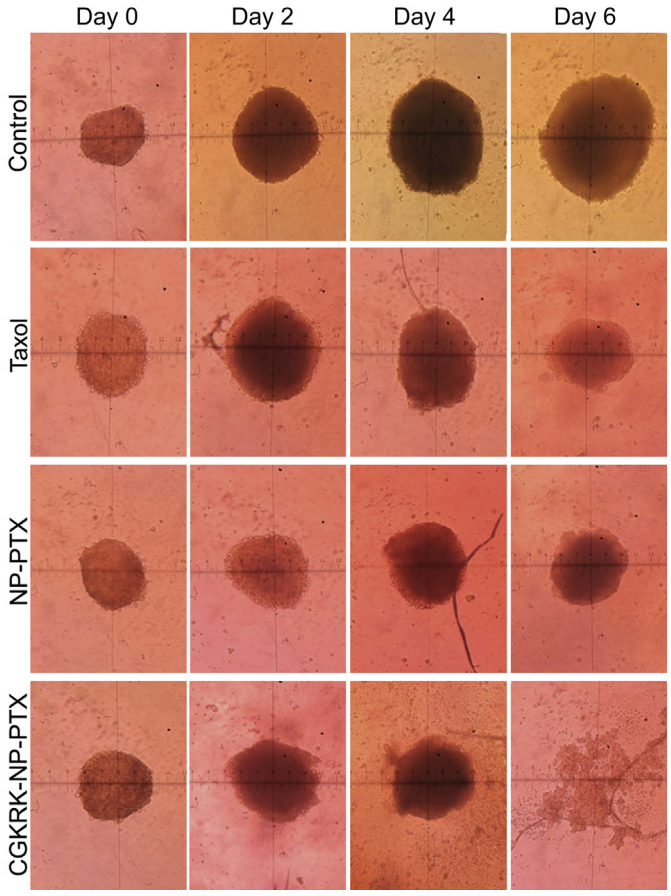

Fig. 10. Morphology of U87MG tumor spheroids treated with serum-free DMEM (A), Taxol® (B), NP-PTX (C) and CGKRK-NP-PTX (D) on day 0, day 2, day 4 and day 6, respectively, at the PTX concentrations 200 ng/ml.

microenvironment provides a greater contribution to antiangiogenic drug resistance. In addition, the tumor mass out of oxygen and nutrient after antiangiogenic therapy would adapt and progress to stages of greater malignancy via a process referred to as "evasive resistance", even in some cases increased lymphatic and distant metastasis. Therefore, so far, tumor angiogenesis blood vessels and tumor cells dual targeting were urgently needed and represented one of the best options to improve the therapeutic efficacy of progression-free or overall survival benefits [41,42].

Many strategies of using tumor angiogenesis blood vessels and tumor cells dual-targeting drug delivery system (DDS) toward the treatment of tumor have been developed over the past few years and showed great combined or synergetic advantages when compared with antiangiogenic therapy alone [24,43,44]. The currently available dual-targeting therapeutics was less than optimal for tumor treatment, mainly owing to the cellular internalization problem contributed by the functional ligand which could result in insufficient intracellular drug concentration. Thus modified a nanoparticulate DDS with a ligand of high dual-targeting property and robust cellular internalization will achieve significant therapeutic efficacy. In this present study, CGKRK peptide, which was reported as a ligand targeted to heparan sulfate that overexpressed on the surface of both neovascular endothelial cells and tumor cells, was utilized as the functional ligand to be conjugated to the surface of PEG-co-PCL nanoparticles. The functionalized CGKRK-NP was expected to achieve tumor angiogenesis blood vessels and tumor cells homing efficacy with high cellular internalization efficiency, and hold a great potential to achieve more efficient anti-cancer activity.

In tumor drug delivery, the size of nanoparticulate DDS needed to be perfectly controlled under 150 nm to meet the demand of enhanced permeability and retention (EPR) effect and decrease blood clearance [45,46]. In our study, the size of PEG-PCL nanoparticle was increased from 103.13 ± 5.7 nm to 117.28 ± 10.42 nm after modification with CGKRK peptide and the size distribution was suitable for anti-tumor drug delivery. The CGKRK conjugation on the surface of CGKRK-NP was confirmed by the elevation of zeta potential from −32.7 ± 5.63 mV to −15.7 ± 3.32 mV and this mainly contributed by the electropositivity of CGKRK peptide.

In vitro PTX release experiment showed a burst release behavior for Taxol® and similar biphases release pattern for the NPs formulations which was in consistent well with previous studies [47]. The release rate of NP formulations in PBS (pH 6.0) was faster than that in PBS (pH 7.4), it was speculated acidic pH could accelerate the degradation of the polymer nanoparticles.

Cellular experiment results showed that a concentration-, temperature- and time-dependent cellular association of CGKRK-NP was achieved on both HUVEC cells and U87MG cells, suggesting a process of active endocytosis. Qualitative (Fig. 2) and quantitative results (Fig. 3) exhibited a significantly higher fluorescence intensity on both HUVEC cells and U87MG cells treated with CGKRK-NP when compared with that of unmodified NP, indicating the specific affinity of CGKRK ligand and heparan sulfate receptor overexpressed on the surface of HUVEC cells and U87MG cells mediated and enhanced cellular endocytosis. Notably, the enhanced cellular uptake of CGKRK-NP over unmodified NP in both HUVEC cells and U87MG cells after quenching by trypan blue was much higher than that before quenching, suggesting that more cellular associated CGKRK-NP was internalized into cellular interior. The increased internalization of nanoparticle, which was contributed by CGKRK peptide, would exhibit great superior in anti-tumor drug delivery by significantly enhancing the intracellular accumulation of drug to kill cancer cells more effectively.

To characterize the endocytosis pathways that involved in the cellular association of CGKRK-NP, both HUVEC cells and U87MG cells were exposed to CGKRK-NP in the presence of various endocytosis inhibitors. As shown in Fig. 4A, the association of CGKRK-NP on HUVEC cells was restricted by microtubules depolymerization agent—colchicines and nocodazole, caveolae-mediated endocytosis pathway inhibitor—filipin and genistein, energy-depletion agent—NaN_3 + dg and lipid raft inhibitor—M-β-CD, suggesting the endocytosis process of CGKRK-NP on HUVEC cells was energy-dependent, lipid raft/caveolae-mediated endocytosis with the involvement of microtubules. In the case of U87MG cells, the association of CGKRK-NP was inhibited by colchicines, filipin, NaN_3 + dg, M-β-CD, nocodazole and Golgi apparatus destroyer—BFA, indicating the involvement of lipid raft/caveolae-mediated endocytosis and Golgi apparatus as well as energy in the process of association of CGKRK-NP in U87MG cells. In addition, pre-added CGKRK peptide significantly inhibited the association of CGKRK-NP in both HUVEC cells and U87MG cells, confirming the contribution of CGKRK peptide modification to enhanced cellular uptake.

The elevated association of CGKRK-NP also resulted in stronger anti-proliferative and apoptosis-induction activity following encapsulation of PTX in both HUVEC cells and U87MG cells. As shown in Fig. 8, the nuclei of HUVEC cells and U87MG cells treated with CGKRK-NP-PTX exhibited much more segmentation and fragmentation compared with that of Taxol® and NP-PTX group after incubation for 48 h. Flow cytometry results also confirmed that nanoparticles with CGKRK peptide modification induced more early and late apoptosis in both HUVEC and U87MG cells. Anti-proliferative analysis showed that the IC50 values of CGKRK-NP-PTX was 1.68, 2 folds lower than that of NP and Taxol® in HUVEC cells and 2.04, 2.4 folds lower than that of NP and Taxol® in U87MG

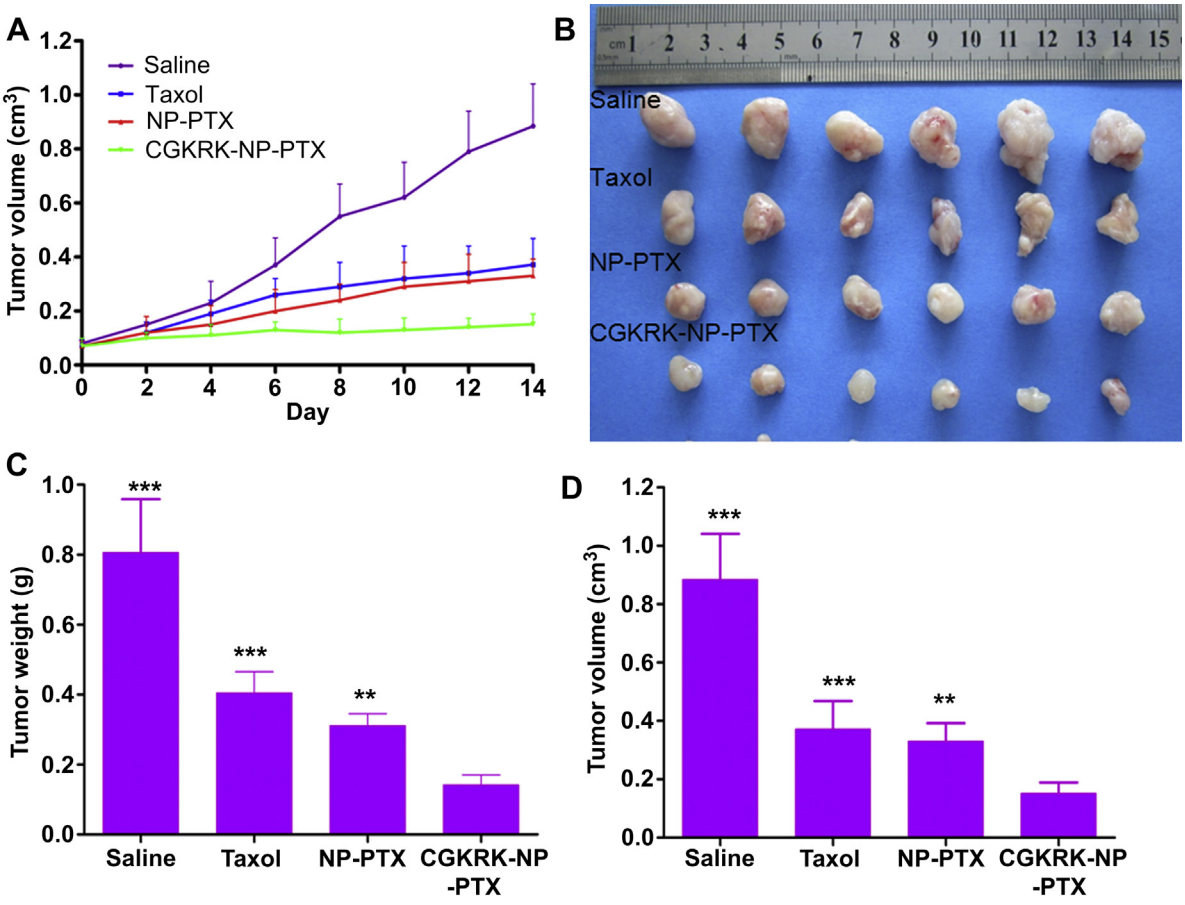

Fig. 11. Anti-tumor growth effects of CGKRK-NP-PTX on nude mice bearing subcutaneous U87MG tumors. Four groups were administrated i.v. with saline, Taxol®, NP-PTX and CGKRK-NP-PTX at PTX dose 5 mg/kg, respectively. The injection was repeated every 2 days for two weeks. Change in body weight of the nude mice bearing subcutaneous U87MG tumors during the 14-day experimental period (A). Tumor morphology and size at the experimental end point (14th day) (B). Tumor weight at the experimental end point (14th day) (C). Tumor volume at the experimental end point (14th day) (D). Data represents mean ± SD, $n = 6$. $^{**}p < 0.01$, $^{***}p < 0.001$ significantly different with that of CGKRK-NP-PTX group.

cells, indicating that enhanced internalization of nanoparticles after functionalization with CGKRK peptide led to much higher intracellular PTX concentration in both cells and thus more efficient anti-cancer activity. Taken these results together, the improved anti-proliferative and induced apoptosis ability was believed to be attributed to the CGKRK peptide, which could bond the receptor of heparan sulfate specifically and robustly and then facilitated the internalization of the PTX formulation into HUVEC cells and U87MG cells. The strong anti-proliferative effect of CGKRK-NP on tumor cells might also prevent local invasion and distant metastasis of tumor cells which often occurred during antiangiogenic therapy alone.

The ex vivo 3D tumor spheroids are not only aggregates of cells in close contact but possess an organized extracellular matrix consisting of fibronectin, laminin, and collagen suggestive of the extracellular matrix of tumors in vivo [48,49]. In addition, the physiologic barriers of tumor spheroids such as high cell density, acidic pH and increased interstitial pressure, increased the difficulty of permeability of anti-tumor drug into solid tumor interior [50,51]. Therefore, the tumor spheroids could be an effective tool to study the performance of DDS. In this study, we employed the ex vivo U87MG tumor spheroids to evaluate the penetration and anti-tumor spheroids growth ability of CGKRK-NP. As shown in Fig. 5, the U87MG tumor spheroids treated with CGKRK-NP exhibited much more extensive fluorescence intensity and deeper penetration depth when compared with that of unmodified NP, indicating the conjugation of CGKRK peptide could facilitate permeation and enrichment of CGKRK-NP in solid tumor. In vitro anti-tumor spheroids growth experiment also confirmed targeting capability of CGKRK-NP with much stronger inhibitory effects on tumor spheroids when compare with Taxol® and NP-PTX (Fig. 10). The improved targeting and penetration ability of CGKRK-NP could enhance the present comprised chemotherapeutic efficacy of anticancer agents and promote a synergetic approach for solid tumor treatment when combine with antiangiogenic therapy.

Xenograft tumors are characterized by synchrony and reproducibility of tumor formation, rapid tumor development, and high penetrance. The use of s.c. models allows for easy tumor visualization, making decisions of treatment initiation and drug application [52,53]. A large panel of xenografts obtained from several types of tumor has been used to compare drug response between the xenograft and the individual patient, resulting in a xenograft potency greater than 90% in predicting correctly the clinical response [54,55]. In this study, xenograft nude mouse models with U87MG cells line implanted in right leg was used for determining the in vivo targeting ability of CGKRK modified nanoparticulate DDS, which provides abundant blood vessels to target and much convenience in evaluating the penetration ability of DDS.

Based on the exciting in vitro cellular results, in vivo NIR imaging experiments was performed to further evaluate the tumor targeting efficacy of CGKRK-NP. As shown in Fig. 6, much stronger fluorescence intensity was achieved at tumor site for CGKRK-NP at all time points when compared with that of unmodified NP. Ex vivo organs imaging showed stronger fluorescence signal in tumor

tissue for CGKRK-NP and was in good consistent with the time-dependent bio-distribution result. These results suggested that CGKRK-NP exhibited a significant superiority in tumor targeting which was mainly contributed by CGKRK-heparan sulfate interaction in vivo than unmodified NP which relied on limited EPR effects to get into tumor site.

In order to study the distribution of CGKRK-NP and unmodified NP in tumor section, the frozen sections of tumor tissue was observed under a laser scanning confocal microscopy. As shown in Fig. 7, it was demonstrated that a low accumulation of NP was achieved and mainly trapped in blood vessels, suggesting the localization of NP at tumor site mostly depended on EPR effects which showed limit extravasation from tumor blood vessels [56]. In contrast, CGKRK-NP exhibited a much stronger fluorescence intensity and more extensive distribution around tumor blood vessels and in tumor foci. It was believed that the accumulation of CGKRK-NP was contributed by the angiogenic blood vessels and tumor cells dual-targeting ability of CGKRK peptide. Functionalization with CGKRK peptide on the surface of nanoparticle could effectively target angiogenic blood vessels, then induce the DDS to extravasate from tumor blood vessels and facilitate DDS to penetrate into tumor parenchyma [26].

For evaluating the anti-tumor efficacy in vivo, the mice bearing subcutaneous U87MG tumors was employed as animal model. The mice were treated with saline, Taxol®, NP-PTX and CGKRK-NP-PTX according to schedules of every two days in two weeks at PTX dose 5 mg/kg. As shown in Fig. 11, the ability to inhibit tumor growth followed the order: CGKRK-NP-PTX > NP-PTX > Taxol® > Saline, strongly suggested the improved accumulation and penetration of CGKRK-NP-PTX at the tumor site led to an anticipated enhanced anti-tumor growth efficacy in vivo.

5. Conclusion

In the present study, we constructed a CGKRK peptide functionalized PEG-co-PCL nanoparticulate DDS to achieve angiogenic blood vessels and tumor cells dual-targeting effect. The CGKRK peptide was conjugated to the surface of PEG-co-PCL nanoparticles via a maleimide-thiol coupling reaction with the particle size of 117.28 ± 10.42 nm. The conjugation of CGKRK peptide was confirmed by increased zeta potential and XPS analysis. Enhanced cellular association was achieved on HUVEC cells and U87MG cells. CGKRK-NP was internalized via an energy-dependent, lipid raft/caveolae-mediated endocytosis with the involvement of microtubules in HUVEC cells and an energy-dependent, lipid raft/caveolae-mediated endocytosis with the participation of Golgi apparatus in U87MG cells. The improved intracellular accumulation of PTX mediated by CGKRK peptide exhibited higher apoptosis induction and anti-proliferative activity. Furthermore, in vitro U87MG tumor spheroids assays showed that CGKRK-NP effectively penetrated into the tumor spheroids and significantly improved the inhibitory effects of PTX on the growth of tumor spheroids. In vivo animal experiment showed that extensive accumulation at tumor site and improved anti-tumor efficacy was achieved for CGKRK-NP. The findings together suggested that CGKRK-NP could be used as an effective tumor angiogenic blood vessels and tumor cells dual-targeting DDS, holding great potential in improving anti-cancer activity and avoiding the drawbacks of antiangiogenic therapy alone.

Acknowledgments

This work was supported by National Key Basic Research Program (2013CB932500), Grants from Shanghai Science and Technology Committee (13NM1400500, 11430702200, 12nm0502000, 12ZR1416300), National Natural Science Foundation of China (81373353), Program for New Century Excellent Talents in University, Innovation Program of Shanghai Municipal Education Commission (12ZZ107), SJTU Funding (AE4160003) and National Science and Technology major Project (2012ZX09304004),

References

[1] Carmeliet P. Angiogenesis in life, disease and medicine. Nature 2005;438:932–6.
[2] van Hinsbergh VW, Collen A, Koolwijk P. Angiogenesis and anti-angiogenesis: perspectives for the treatment of solid tumors. Ann Oncol 1999;10(Suppl. 4):60–3.
[3] Carmeliet P, Jain RK. Angiogenesis in cancer and other diseases. Nature 2000;407:249–57.
[4] Folkman J. The role of angiogenesis in tumor growth. Semin Cancer Biol 1992;3:65–71.
[5] Folkman J. Role of angiogenesis in tumor growth and metastasis. Semin Oncol 2002;29:15–8.
[6] Shojaei F. Anti-angiogenesis therapy in cancer: current challenges and future perspectives. Cancer Lett 2012;320:130–7.
[7] Bai F, Wang C, Lu Q, Zhao M, Ban FQ, Yu DH, et al. Nanoparticle-mediated drug delivery to tumor neovasculature to combat P-gp expressing multidrug resistant cancer. Biomaterials 2013;34:6163–74.
[8] Ellis LM, Hicklin DJ. VEGF-targeted therapy: mechanisms of anti-tumour activity. Nat Rev Cancer 2008;8:579–91.
[9] Kane RC, Farrell AT, Saber H, Tang S, Williams G, Jee JM, et al. Sorafenib for the treatment of advanced renal cell carcinoma. Clin Cancer Res 2006;12:7271–8.
[10] Goodman VL, Rock EP, Dagher R, Ramchandani RP, Abraham S, Gobburu JV, et al. Approval summary: sunitinib for the treatment of imatinib refractory or intolerant gastrointestinal stromal tumors and advanced renal cell carcinoma. Clin Cancer Res 2007;13:1367–73.
[11] Hurwitz H, Fehrenbacher L, Novotny W, Cartwright T, Hainsworth J, Heim W, et al. Bevacizumab plus irinotecan, fluorouracil, and leucovorin for metastatic colorectal cancer. N Engl J Med 2004;350:2335–42.
[12] Jain RK, Carmeliet P. SnapShot: tumor angiogenesis. Cell 2012;149:1408-e1.
[13] Mullard A. 2012 FDA drug approvals. Nat Rev Drug Discov 2013;12:87–90.
[14] Casanovas O, Hicklin DJ, Bergers G, Hanahan D. Drug resistance by evasion of antiangiogenic targeting of VEGF signaling in late-stage pancreatic islet tumors. Cancer Cell 2005;8:299–309.
[15] Shojaei F, Wu X, Malik AK, Zhong C, Baldwin ME, Schanz S, et al. Tumor refractoriness to anti-VEGF treatment is mediated by CD11b+Gr1+ myeloid cells. Nat Biotechnol 2007;25:911–20.
[16] Shojaei F, Wu X, Qu X, Kowanetz M, Yu L, Tan M, et al. G-CSF-initiated myeloid cell mobilization and angiogenesis mediate tumor refractoriness to anti-VEGF therapy in mouse models. Proc Natl Acad Sci U S A 2009;106:6742–7.
[17] Crawford Y, Kasman I, Yu L, Zhong C, Wu X, Modrusan Z, et al. PDGF-C mediates the angiogenic and tumorigenic properties of fibroblasts associated with tumors refractory to anti-VEGF treatment. Cancer Cell 2009;15:21–34.
[18] Shojaei F, Lee JH, Simmons BH, Wong A, Esparza CO, Plumlee PA, et al. HGF/c-Met acts as an alternative angiogenic pathway in sunitinib-resistant tumors. Cancer Res 2010;70:10090–100.
[19] Miller KD, Sweeney CJ, Sledge Jr GW. Can tumor angiogenesis be inhibited without resistance? EXS 2005:95–112.
[20] Bergers G, Hanahan D. Modes of resistance to anti-angiogenic therapy. Nat Rev Cancer 2008;8:592–603.
[21] Paez-Ribes M, Allen E, Hudock J, Takeda T, Okuyama H, Vinals F, et al. Antiangiogenic therapy elicits malignant progression of tumors to increased local invasion and distant metastasis. Cancer Cell 2009;15:220–31.
[22] Ebos JM, Lee CR, Cruz-Munoz W, Bjarnason GA, Christensen JG, Kerbel RS. Accelerated metastasis after short-term treatment with a potent inhibitor of tumor angiogenesis. Cancer Cell 2009;15:232–9.
[23] Potente M, Gerhardt H, Carmeliet P. Basic and therapeutic aspects of angiogenesis. Cell 2011;146:873–87.
[24] Pastorino F, Brignole C, Di Paolo D, Nico B, Pezzolo A, Marimpietri D, et al. Targeting liposomal chemotherapy via both tumor cell-specific and tumor vasculature-specific ligands potentiates therapeutic efficacy. Cancer Res 2006;66:10073–82.
[25] Hoffman JA, Giraudo E, Singh M, Zhang L, Inoue M, Porkka K, et al. Progressive vascular changes in a transgenic mouse model of squamous cell carcinoma. Cancer Cell 2003;4:383–91.
[26] Agemy L, Friedmann-Morvinski D, Kotamraju VR, Roth L, Sugahara KN, Girard OM, et al. Targeted nanoparticle enhanced proapoptotic peptide as potential therapy for glioblastoma. Proc Natl Acad Sci U S A 2011;108:17450–5.
[27] Jarvinen TA, Ruoslahti E. Molecular changes in the vasculature of injured tissues. Am J Pathol 2007;171:702–11.
[28] Yao XL, Yoshioka Y, Ruan GX, Chen YZ, Mizuguchi H, Mukai Y, et al. Optimization and internalization mechanisms of PEGylated adenovirus vector with targeting peptide for cancer gene therapy. Biomacromolecules 2012;13:2402–9.
[29] Richard JP, Melikov K, Vives E, Ramos C, Verbeure B, Gait MJ, et al. Cell-penetrating peptides. A reevaluation of the mechanism of cellular uptake. J Biol Chem 2003;278:585–90.

[30] Hu Q, Gu G, Liu Z, Jiang M, Kang T, Miao D, et al. F3 peptide-functionalized PEG-PLA nanoparticles co-administrated with tLyp-1 peptide for anti-glioma drug delivery. Biomaterials 2013;34:1135–45.
[31] Hu Q, Gao X, Gu G, Kang T, Tu Y, Liu Z, et al. Glioma therapy using tumor homing and penetrating peptide-functionalized PEG-PLA nanoparticles loaded with paclitaxel. Biomaterials 2013;34:5640–50.
[32] Gu G, Xia H, Hu Q, Liu Z, Jiang M, Kang T, et al. PEG-co-PCL nanoparticles modified with MMP-2/9 activatable low molecular weight protamine for enhanced targeted glioblastoma therapy. Biomaterials 2013;34:196–208.
[33] Folkman J. Anti-angiogenesis: new concept for therapy of solid tumors. Ann Surg 1972;175:409–16.
[34] Brem S, Cotran R, Folkman J. Tumor angiogenesis: a quantitative method for histologic grading. J Natl Cancer Inst 1972;48:347–56.
[35] Escudier B, Eisen T, Stadler WM, Szczylik C, Oudard S, Siebels M, et al. Sorafenib in advanced clear-cell renal-cell carcinoma. N Engl J Med 2007;356:125–34.
[36] Motzer RJ, Hutson TE, Tomczak P, Michaelson MD, Bukowski RM, Rixe O, et al. Sunitinib versus interferon alfa in metastatic renal-cell carcinoma. N Engl J Med 2007;356:115–24.
[37] Shojaei F, Ferrara N. Role of the microenvironment in tumor growth and in refractoriness/resistance to anti-angiogenic therapies. Drug Resist Updat 2008;11:219–30.
[38] Crawford Y, Ferrara N. Tumor and stromal pathways mediating refractoriness/resistance to anti-angiogenic therapies. Trends Pharmacol Sci 2009;30:624–30.
[39] Blagosklonny MV. Antiangiogenic therapy and tumor progression. Cancer Cell 2004;5:13–7.
[40] Ebos JM, Kerbel RS. Antiangiogenic therapy: impact on invasion, disease progression, and metastasis. Nat Rev Clin Oncol 2011;8:210–21.
[41] Luo LM, Huang Y, Zhao BX, Zhao X, Duan Y, Du R, et al. Anti-tumor and anti-angiogenic effect of metronomic cyclic NGR-modified liposomes containing paclitaxel. Biomaterials 2013;34:1102–14.
[42] Yu DH, Ban FQ, Zhao M, Lu Q, Lovell JF, Bai F, et al. The use of nanoparticulate delivery systems in metronomic chemotherapy. Biomaterials 2013;34:3925–37.
[43] Hare JI, Moase EH, Allen TM. Targeting combinations of liposomal drugs to both tumor vasculature cells and tumor cells for the treatment of HER2-positive breast cancer. J Drug Target 2013;21:87–96.
[44] Li Y, Lei Y, Wagner E, Xie C, Lu W, Zhu J, et al. Potent retro-inverso D-peptide for simultaneous targeting of angiogenic blood vasculature and tumor cells. Bioconjug Chem 2013;24:133–43.
[45] Li SD, Huang L. Pharmacokinetics and biodistribution of nanoparticles. Mol Pharm 2008;5:496–504.
[46] Alexis F, Pridgen E, Molnar LK, Farokhzad OC. Factors affecting the clearance and biodistribution of polymeric nanoparticles. Mol Pharm 2008;5:505–15.
[47] Zeng N, Hu Q, Liu Z, Gao X, Hu R, Song Q, et al. Preparation and characterization of paclitaxel-loaded DSPE-PEG-liquid crystalline nanoparticles (LCNPs) for improved bioavailability. Int J Pharm 2012;424:58–66.
[48] Minchinton AI, Tannock IF. Drug penetration in solid tumours. Nat Rev Cancer 2006;6:583–92.
[49] Davies CD, Muller H, Hagen I, Garseth M, Hjelstuen MH. Comparison of extracellular matrix in human osteosarcomas and melanomas growing as xenografts, multicellular spheroids, and monolayer cultures. Anticancer Res 1997;17:4317–26.
[50] Hirschhaeuser F, Menne H, Dittfeld C, West J, Mueller-Klieser W, Kunz-Schughart LA. Multicellular tumor spheroids: an underestimated tool is catching up again. J Biotechnol 2010;148:3–15.
[51] Jiang X, Xin H, Gu J, Xu X, Xia W, Chen S, et al. Solid tumor penetration by integrin-mediated pegylated poly(trimethylene carbonate) nanoparticles loaded with paclitaxel. Biomaterials 2013;34:1739–46.
[52] Kelland LR. Of mice and men: values and liabilities of the athymic nude mouse model in anticancer drug development. Eur J Cancer 2004;40:827–36.
[53] Sausville EA, Burger AM. Contributions of human tumor xenografts to anticancer drug development. Cancer Res 2006;66:3351–4 [discussion 4].
[54] Fiebig HH, Maier A, Burger AM. Clonogenic assay with established human tumour xenografts: correlation of in vitro to in vivo activity as a basis for anticancer drug discovery. Eur J Cancer 2004;40:802–20.
[55] Luconi M, Mannelli M. Xenograft models for preclinical drug testing: implications for adrenocortical cancer. Mol Cell Endocrinol 2012;351:71–7.
[56] Fang J, Nakamura H, Maeda H. The EPR effect: unique features of tumor blood vessels for drug delivery, factors involved, and limitations and augmentation of the effect. Adv Drug Deliv Rev 2011;63:136–51.